R. A. Bortolozzi and M. G. Chiovetta*

Three-Phase Model of a Fluidized-Bed Catalytic Reactor for Polyethylene Synthesis

DOI 10.1515/ijcre-2015-0002

Abstract: A mathematical model of a bubbling fluidized-bed reactor for the production of polyolefins is presented. The model is employed to simulate a typical, commercial-scale reactor where the synthesis of polyethylene using supported catalysts is carried out. Results are used to follow the evolution of temperature within the reactor bed to avoid conditions producing polymer degradation. The fluidized bed is modeled as a heterogeneous system with a bubble gas phase and a solid-particle emulsion. The catalyst active sites are considered located within a growing, solid, ever changing particle composed of the support, the catalyst and the polymer being produced. The model sees the reactor as a three phase complex: (a) the bubble phase, transporting most of the gas entering the reactor; (b) the solid-particle phase, where polymerization takes place; and (c) the interstitial-gas phase among solid particles. Both gaseous phases move continuously upward, with different velocities, and are modeled as plug flows. For the solid-particle phase, modeling alternatives are explored, ranging from a descending plug-flow limiting case to the opposite extreme of a perfectly mixed tank related to the particle drag-effect the rising bubble produces in the bed. In the scouting process between these limits instabilities are predicted by the model. The most realistic representation of the bed is that of the two gas phases moving upward in two plug-flow patterns and the solids moving with ascending and descending trajectories due to back-mixing.

Keywords: olefin polymerization, mathematical model, fluidized-bed reactor, three-phase model, back-mixing, instability, numerical scouting

***Corresponding author: M. G. Chiovetta,** Instituto de Desarrollo Tecnológico para la Industria Química – INTEC (Universidad Nacional del Litoral – CONICET), Güemes 3450, S3000GLN Santa Fe, Argentina, E-mail: mchiove@intec.unl.edu.ar

R. A. Bortolozzi, Instituto de Desarrollo Tecnológico para la Industria Química – INTEC (Universidad Nacional del Litoral – CONICET), Güemes 3450, S3000GLN Santa Fe, Argentina, E-mail: rabor@santafe-conicet.gov.ar

1 Introduction

Poly-ethylene and – propylene are the thermoplastics with the world's largest production. Installed capacities are in the order of 100 million tons/year and production values in the order of 140,000 million dollars/year. More than 40 million tons/year are associated with monomer schemes in the gas phase. In turn, the majority of these corresponds to plants in which the reactor is of the fluidized-bed type.

In particular, for one of the most widely used process to produce polyethylene – UNIPOL PE, Univation Technologies- more than 100 production lines are currently operating in the world, with an average capacity of the order of 175,000 tonnes of polyethylene/year per product line (Univation, 2013). This fact has led the fluidized-bed technology to be considered the dominant in the field of gas-phase monomer polyolefins. By way of example, in Argentina the installed capacity for polyolefin production is in the order of 750,000 tons per year, with approximately 35% corresponding to processes with gaseous monomers, and 65% of these processes involving fluidized-bed reactors.

Around 90% of the world production of polyolefins corresponds to reactions with heterogeneous catalysts, mainly supported, with active sites grouped into two broad categories: (1) Cr-based and Ziegler-Natta catalysts, and (2) metallocene catalysts. Catalysts in group (1) were originated in the 1960s and now dominate the market through successive evolutions.

Metallocene catalysts (group 2) represent the advanced technology and since the early 90 (Kaminsky and Renner 1993) have been gradually entering the industrial production scene. Metallocene polyolefins show qualities some of which are impossible or difficult to obtain with category (1) catalysts. Additionally, metallocene activities are higher and they are capable of producing polymer chains with controlled tacticity, even piecewise within a single molecule.

Gas phase processes, while dominating the industrial market, present considerable difficulties in the administration of the energy released during the polymerization. This circumstance becomes more important when considering the higher activity and, therefore, the greater energy release rate in metallocene systems.

The global picture shows a trend to adapt the existing production plants to the new metallocene catalysts including the enhancement produced by the addition of condensable monomers and other condensable species. This situation has generated a growing demand for suitable reactor mathematical models for these newer conditions, in order to find adequate representations to improve the analysis and design of equipment. In the literature, a variety of mathematical models for fluidized-bed reactors (Mahecha-Botero et al. 2009) have been published. In general, these models are complex because they involve a set of concurrent events, which are difficult to describe due to the large number of necessary equations, the strong coupling among them and the nonlinear nature of the problem.

In this paper, a three-phase model for the analysis of a fluidized-bed reactor with metallocene catalysts and the results of its application to typical cases are presented.

2 Mathematical model of the fluidized-bed reactor

2.1 Three-phase model

In the version of the model presented in previous works by Bortolozzi and Chiovetta (2006, 2007), a two-phase model was used to describe the physical system, one phase being the bubble phase whilst the other is the emulsion phase. The latter was considered a pseudo-continuum containing particles and interstitial gas (see, for example, Kiashemshaki et al. 2006).

Dompazis et al. (2008) present a detailed description of the phenomena taking place in a reactor modeled using cylindrical sections, in one of the most complete mathematical schemes in the literature. It is based on a two phase/compartment (emulsion and bubble-wake) distribution for each section in the reactor, gravity, buoyancy and drag forces acting on the particles.

In the model presented herein, the representation closest to the conditions suggested by experimental evidence described in the literature corresponds to a scheme in which the gas in the bubble phase moves in plug-flow conditions while the emulsion phase is regarded as perfectly mixed. This simplified representation is very extreme, and introduces into the model certain conditions that generate instabilities during its numerical solution. However, this unstable behavior is consistent with the physical instability of the system when it is considered that the reactant emulsion is a perfectly mixed reactor. For this model, the reactor operating point at a temperature necessary to obtain an acceptable production level lies in the unstable zone.

All these elements suggest that the model should be modified, in order to consider, at least for the emulsion, a behavior with characteristics intermediate between the plug-flow and the perfect-mix conditions. This can be achieved if the emulsion is represented as split into two phases: the interstitial gas, which maintains a behavior close to that of a plug-flow, and the solid particles, with upward and downward movements, related to the bubble motion in the bed, which produces a mixing effect in the axial direction. Accordingly, a new scheme for the reactor is developed considering three phases: the gas bubbles, the interstitial gas and the solid particles (Bortolozzi and Chiovetta 2010). The gas bubbles are considered moving virtually as a plug flow, and so is the interstitial gas. However, velocities in the upward flow are clearly different: the ratio of bubble to interstitial-gas velocities correspond to the case of fast bubbles (Kunii and Levenspiel 1991). The bubble is surrounded by a cloud, which thickness is not very significant due to the relatively high bubble velocity upward. However, the presence of the cloud is important for the transfer mechanisms between the gas in the bubble and the interstitial gas. These mechanisms involve the convective transport of energy and mass between both gases, in addition to the diffusive contribution which, for the cases studied, is not relevant. The solid particles fluidized by the gas stream have a complex behavior. Indeed, the gas that rises as bubbles produces an entrainment of solid particles in the wake following the bubbles. When these particles exit the wake, or reach the top of the bed, they tend to fall toward the bottom of the reactor. Thus, two streams of solid particles are established: a rising stream, due to the entrainment of bubbles, and a descending stream, with a waterfall-type behavior. Throughout this ascending-descending path, particles grow due to the chemical reactions leading to the synthesis of the polymer in the support/catalyst/polymer matrix. The solid extraction system of the reactor, located near the bottom of the main vessel, classifies particles by size, and returns to the reactor small particles, so that the net effect is an output of sufficiently large size particles. As in the two-phase model presented in previous works, the bed is considered divided into cylindrical slices of equal size, named sections, vertically spanning the bed-height. A simplified schematic of a generic section is presented in Figure 1. Phase movements are indicated with vertical

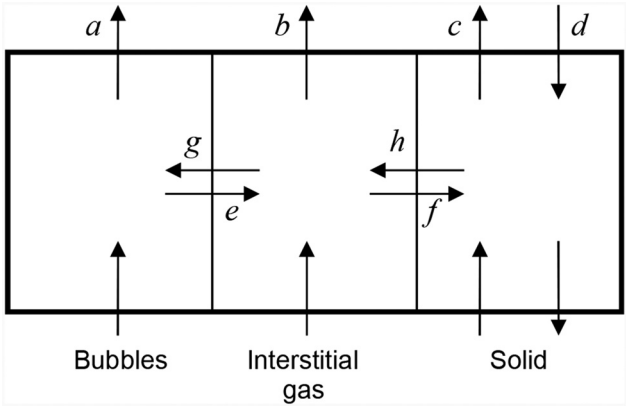

Figure 1: Scheme of a generic section of the reactor.

arrows and the exchange of mass and heat that occurs between them, with horizontal arrows. This scheme corresponds to any intermediate section in the bed.

In summary, as depicted in Figure 1, this new scheme for the system model provides three upstream flows, two gaseous and one of solid particles (*a*, *b* and *c* respectively, in Figure 1) and one downstream flow with only solid particles (*d*). Monomer mass transfer occurs from the gas to the solid (*e* and *f*), while heat is transferred (*g* and *h*) in the opposite direction thereto.

To complete the representation, the gas flow entering the reactor is considered split into two streams (bubbles and interstitial gas) as soon as it enters the bed through the bottom of the vessel. The exit of the solid product is considered located at the lower zone of the bed, with the unreacted gas stream leaving the reactor through the top.

In each section, rising particles carried by the wake of the bubbles, come from low-lying portions of the bed, where the temperature is lower. Therefore these particles tend to cool the higher sections. Conversely, descending particles move down from regions of higher temperature and, consequently, tend to heat lower portions. This double movement produces an effect of axial mixing, which smooths the gradients of temperature and significantly changes the trend observed when considering a purely plug flow behavior. Indeed, if each phase is modeled as a plug flow upward, the temperature gradients increase along the gas path, showing a very steep slope in the upper region of the reactor. As stated in the literature (Jenkins et al. 1986), evidence would indicate otherwise: the greatest temperature variations seem to occur in the lower portion of the bed, near the gas entrance to the reactor.

When both ascending and descending flows are calculated for the solid, the corresponding velocities for said flows result very low. Hence, no correction for the average velocity field of the interstitial gas appears necessary. Additionally, when the ascending particle flow in the bubble wake is analyzed, it is possible to calculate that, for the maximum drag considered in this work, the portion of bed particles in said flow does not exceed 13%. This figure indicates that it has no major influence on the gas flow. Because of these reasons, no correction was introduced to the basic fluid-mechanic equations in a typical fluidized bed that are used in the model.

Each section representing the bed, as mentioned earlier, is modeled as a reactor sub-system that exchange mass and heat with adjacent sections. The mechanism of back mixing that occurs in the phase of solid particles is quantified in the model by a mixing factor f_A, defined as follows:

$$f_A = \frac{\dot{m}_s}{\dot{m}_b} \tag{1}$$

where $\dot{m}_s$ is the mass flow rate of solid particles that are entrained in the gas stream formed by the rising bubbles and whose mass flow rate is $\dot{m}_b$. Both amounts are expressed in kg/s. When f_A is zero, no effect of back mixing is considered and the phase moves under plug flow conditions. Conversely, when this factor is not null, mixing is regarded as existing. If f_A increases, the phase approaches the perfect mixing conditions. Theoretically, this situation corresponds to a case when the upward-downward movement of the particles is so intense that causes uniformity of the phase properties, especially the temperature.

In this work we consider an intermediate situation: taking into account that industrial reactors have ratios L/D much greater than 1, the application of the hypothesis of perfect mixing is unrealistic. Nonetheless, existing fluidized-bed mixing effects discourage the application of a purely plug-flow scheme.

The bed is considered divided into a number of sections designated as N_{sec}, each containing all three phases presented above. The two upward gas streams are modeled without back mixing, so that the succession of sections represents a plug flow behavior if N_{sec} is large enough. Instead, in the solid phase, the mixture of particles in the axial direction results in an intermediate behavior between the plug-flow and perfect-mix models.

2.2 Fluid-mechanics

Fluidized-bed reactors for industrial production of polyethylene operate in bubbling flow regime (Choi and Ray 1985; McAuley et al. 1994; Kou et al. 2005). For the

Table 1: Dimensions of the reactor.

Bed height, L (m)	12
Diameter, D (m)	3.6
Cross area, A_T (m^2)	10.18
Bed volume, V_R (m^3)	122

simulations in this work, a reactor with the typical dimensions in Table 1 is modeled.

Due to the reactor geometry and the design of the gas distributor placed at the bottom of the bed, large bubbles are produced.

The model considers that a fraction of the gas flow generates minimum-fluidization conditions in the emulsion, while the remaining flow passes through the bed in the form of bubbles (Kunii and Levenspiel 1991).

In a fluidized bed, consideration should be given to: a) the absolute velocity of the bubbles u_b, b) the superficial velocity of the gas u_0, c) the minimum fluidization velocity u_{mf}, and d) the relative velocity of bubble rising u_{br}. The equation that relates these velocities is (Kunii and Levenspiel 1991):

$$u_b = u_0 - u_{mf} + u_{br} \tag{2}$$

being,

$$u_{br} = 0.711(g d_b)^{1/2} \tag{3}$$

where d_b is the average bubble diameter along the reactor bed.

The mass balance equations use the bubble fraction in the bed as a parameter; its average value is given by:

$$\delta = \frac{u_0 - u_{mf}}{u_b - u_{mf}} \tag{4}$$

2.3 Mass and energy balances

Mass and energy balances are performed for both the gas and solid flows in the three phases present after the total flow of gas splits. Balances are written for all of the reactor sections, including a term for each contributing effect.

For the bubble gas flow in a generic section, inlet and outlet gas streams are considered, with ethylene being transferred into the interstitial gas.

For the same section, the interstitial gas is affected by two transfers: (a) the flow of incoming ethylene and other species from the bubble, and (b) the flow entering the particle phase.

Finally, the solid (particle) phase in the section sees an ethylene and other molecules flow from the interstitial gas, while reactants are consumed in the active sites within the support/catalyst/polymer particles to produce polyethylene.

Considering the particle motion, the balance for the solid-phase in a generic section involves input and output streams through the section top and bottom: due to mixing and drag, ascending and descending currents of particles are present, according to the scheme in Figure 1, where mass and energy flows entering and leaving a generic section of the reactor are shown.

In the first and last sections of the bed, corresponding to the bottom and the top of the reactor respectively, the situation for the solid phase is different from any other section: a) the section above the gas distributor at the inlet to the reactor has no solids entering from the bottom, and the outlet of the reaction product, which is continuously withdrawn from the reactor (Figure 2(a)) is located here; b) in the last section, at the top, which corresponds to the physical end of the bed, no solid is considered leaving the reactor and, hence, all particles entering the section from below should exit through the same border (Figure 2(b)).

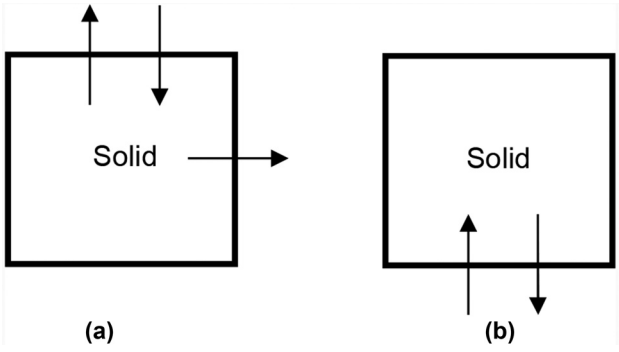

Figure 2: (a) Scheme of the lower section of the reactor (solid phase). (b) Scheme of the upper section of the reactor (solid phase).

For all sections, the solid upward flow is due to the entrainment of particles by the bubbles, and, as previously stated, is described by f_A, a coefficient that, expressing the relation between the gas flow rate and the amount of entrained solid, reduces the overall number of variables for each section by establishing a link between the two flows.

Based on the foregoing analysis, balance equations of ethylene in the gas bubbles, the interstitial gas and the solid particles for the generic section shown in Figure 1 are:

$$u_b\delta\left(\rho_{et}^{i}-\rho_{et}^{o}\right)-K_{big}\left(\rho_{et}^{o}-\hat{\rho}_{et}^{o}\right)L_S\delta=0 \tag{5}$$

$$u_{mf}\left(\hat{\rho}_{et}^{i}-\hat{\rho}_{et}^{o}\right)(1-\delta)+K_{big}\left(\rho_{et}^{o}-\hat{\rho}_{et}^{o}\right)L_S\delta-k^s\hat{\rho}_{et}^{o}L_S(1-\delta)=0 \tag{6}$$

$$\dot{m}_{inf}^{i}+\dot{m}_{sup}^{i}-\dot{m}_{inf}^{o}-\dot{m}_{sup}^{o}+k^s\hat{\rho}_{et}^{o}A_tL_S(1-\delta)=0 \tag{7}$$

In eqs (5), (6) and (7), superscripts (*i*) and (*o*) refer to flows entering and leaving the section considered, respectively. The first term in eq. (5) involves the velocity of the bubble phase, evaluated with eqs (2) and (3) with the average bubble diameter. The fraction of bubbles in the bed is calculated using eq. (4) and the minimum fluidization velocity is estimated using the average diameter of particles and the equations presented in Grosso and Chiovetta (2005). Solid balance (7) involves mass flow rates of polyethylene. Equations (6) and (7) involve a chemical reaction term, which includes the first-order reaction rate constant k^s. This parameter is expressed as:

$$k^s=f_ck_0^s=f_cAe^{-E/RT} \tag{8}$$

where temperature effects in the section are considered through an Arrhenius-type function. To take into account several catalyst activities, a kinetic factor f_c is defined. Its value is 1 when the rate constant takes the value indicated in Table 2, being $T=T_i$.

Table 2: Parameters and properties at the base-case operating conditions for the reactor.

Parameter/Property	Value
r_g (kg/m^3)	24.72
r_s (kg/m^3)	570
Cp_g (J/kg K)	1,730
k_g (W/m K)	0.0269
D_g (m^2/s)	8.65×10^{-7}
ΔH_R (J/kg) @ 333 K	-3.142×10^{6}
T_i (K)	333
k_o^s (1/s) @ 333 K	1.273×10^{-3}
d_p (m)	2×10^{-3}
d_b (m)	0.408
e_{mf} (–)	0.39
u_o (m/s)	0.70
u_{mf} (m/s)	0.119

Equations (5) and (6) are similar to the two-phase model presented in earlier work (Chiovetta and Bortolozzi 2009) although modified to account for the back mixing effects and the new phase distribution. Equation (7) corresponds to the solid motion and involves, in general, two input streams (upper and lower) and two output streams (upper and lower). The remaining term in the equation represents the generation of polymer by chemical reaction. In the bed extreme sections, both lower and upper, some of the solid flows are not present (Figure 2(a) and (b)) and consequently the treatment is different from that in any intermediate section.

An important issue is that concerning the fact that, under steady-state conditions, the number of particles in the reactor, usually in of the order of 10^{10}, must remain constant. Production is obtained only through particle size increase, going from the value that corresponds to the initial support/catalyst pellets (small particles of about 100 microns in diameter) to the size of those effectively removed from the reactor (large particles of about 30 times de initial diameter). The number of catalyst particles entering per unit time equals the number of product particles leaving the bottom of the reactor per unit time (around 500,000 particles per second in a typical case).

The energy balance in the gas also involves input and output terms, transfer across the interfaces, and heat generated by the polymerization reaction, which should be removed from the system by the gas stream as sensible heat. The energy balance equations in the gas of each phase and solid particles in the section considered are:

$$u_bA_T\delta\sum_j\rho_j^iC_{Pj}\left(T^i-T^o\right)+H_{big}A_TL_S\delta\left(\hat{T}^o-T^o\right)=0 \tag{9}$$

$$u_{mf}A_T(1-\delta)\sum_j\hat{\rho}_j^iC_{Pj}\left(\hat{T}^i-\hat{T}^o\right)-H_{big}A_TL_S\delta\left(\hat{T}^o-T^o\right)+hA_{sg}\left(\bar{T}^o-\hat{T}^o\right)=0 \tag{10}$$

$$\dot{m}_{inf}^{i}C_{Ps}\left(\bar{T}_{inf}^{i}-\bar{T}^o\right)+\dot{m}_{sup}^{i}C_{Ps}\left(\bar{T}_{sup}^{i}-\bar{T}^o\right)-hA_{sg}\left(\bar{T}^o-\hat{T}^o\right)+k^s\hat{\rho}_{et}^{o}A_TL_S(1-\delta)(-\Delta H_R)=0 \tag{11}$$

In the energy balance of the solid phase the temperature of the particles contained in the section considered is taken as the reference temperature for the enthalpy calculations, so that the output stream terms are rendered null in this balance. In addition, some terms of lower order were neglected, such as the change of internal energy by viscous dissipation and by expansion of the gas phase.

In the balance equations, mass and heat transfer coefficients are calculated for the average diameters of bubbles and particles. The first one is modeled by the expression (Kunii and Levenspiel 1991),

$$K_{big}=4.5\frac{u_{mf}}{d_b}+5.85\frac{D_g^{1/2}g^{1/4}}{d_b^{5/4}} \tag{12}$$

The heat transfer is described through the coefficient (Kunii and Levenspiel 1991),

$$H_{big} = 4.5\frac{u_{mf}}{d_b}\rho_g C_{Pg} + 5.85\frac{\left(k_g\rho_g C_{Pg}\right)^{1/2} g^{1/4}}{d_b^{5/4}} \tag{13}$$

Both expressions describe heat and mass transfer between the bubbles and the interstitial gas in contact with them and, hence, correspond to a typical gas-gas situation. They contain both a convective and a diffusive contribution.

Other parameters and properties involved in eqs (12) and (13) are shown in Table 2. For most of them, values are taken from Chiovetta and Bortolozzi (2009), with the rest coming from Kunii and Levenspiel (1991). The thermophysical properties of the compounds are taken from Reid et al. (1987). The reference value of the reaction rate specific constant that is included in Table 2 corresponds to the temperature T_i = 333 K. The interface area A_{sg} included in eq. (11), through which the heat is transferred from the solid to the interstitial gas, is the sum of the surface of all particles contained in the section.

The heat transfer coefficient h for the energy transfer between the solid particle and the surrounding fluid is computed using the correlation of Wakao and Kaguei (1982):

$$Nu = 2 + 1.1Pr^{1/3}Re^{0.6} \tag{14}$$

$$h = Nu\left(\frac{k_g}{d_p}\right) \tag{15}$$

For the base-case conditions, h results equal to 609 W/(m^2 K).

Mass and energy balances are resolved numerically. The matrices in the nonlinear system arising from the coupling of thermal and concentration effects through the chemical reaction term are solved. Values of temperature and concentration are evaluated as outputs of each of the reactor sections. Starting at the bottom section and progressing upwards calculations lead to the concentration and temperature values in the gas stream leaving the top of the reactor.

3 Solving the mathematical model

The mathematical model is used to simulate the behavior of a typical industrial fluidized-bed reactor with the dimensions in Table 1 Simultaneous solving of eqs (5) to (11) computes the values of concentrations and temperatures in each section of the reactor, through the following sequence:

(a) First, fluid-dynamic parameters involved in the balance equations are evaluated. An average particle size is established following the calculations based on residence time data and initial particle size at the reactor catalyst-feed point in Grosso and Chiovetta (2005). With data corresponding to properties of the gas entering the reactor, the minimum fluidization velocity (Lucas et al. 1986; Chiovetta and Bortolozzi 2009) is calculated employing the base-case parameters in Table 2.

(b) Using data from the gas flow and the diameter and number of holes in the distributor, the evolution of bubble size d_b is calculated as a function of bed height from its base to the top (Darton et al. 1977). Again, conditions for the reactor operations are taken from Table 2. With this bubble size distribution, the average bubble diameter along the reactor height is calculated and the result shown in Table 2.

(c) The average bubble diameter d_b is then used to calculate the heat and mass transfer coefficients in eqs (12) and (13), the fraction of bubbles δ in eq. (4), and the bubble phase velocity u_b eqs (2) and (3) according to the expressions proposed by Kunii and Levenspiel (1991).

(d) The mass and energy balances are treated as sets of simultaneous algebraic equations coupled through the chemical reaction term, a function of temperature. The resulting matrix is conveniently rearranged to be solved via a numerical scheme performing the matrix inversion to obtain the values of concentration of ethylene and temperatures of the phases present in each section. The procedure involves an iterative process with successive approximations for the solution of the mass and energy balances, until a convergence criterion is satisfied. A relative error (the absolute value of the difference between two successive concentrations or temperatures divided by the last obtained) of 10^{-3} was considered acceptable.

4 Results and discussion

Model predictions within the domain of feasible values for the reactor main parameters are plotted in Figure 3. Results show the productivity of reactor with the base-case parameters, modeled as a function of the number of sections in the bed and the mixing factor.

For a given catalyst activity, established by a number of active sites in the particle considered a constant in the mathematical scheme, reactor productivity measured in kilograms of polyethylene synthesized per hour and per

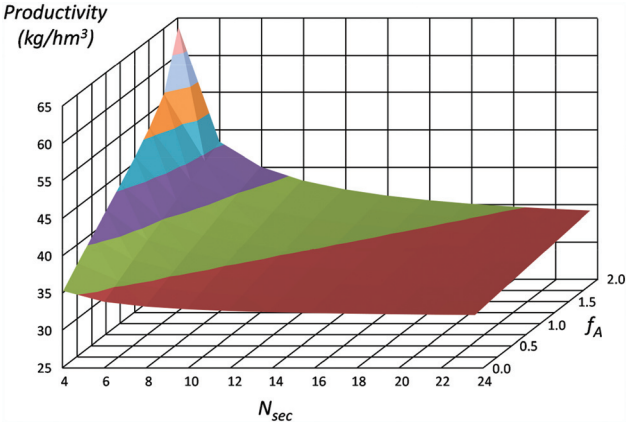

Figure 3: Polyethylene productivity (kg/h m^3) vs. number of sections and mixing factor, for $f_c = 1$.

cubic meter decreases when modeling with more sections and increases for higher values of f_A.

To explain these effects, the influence of N_{sec} and f_A is related to the fact that when they are set in a manner such that the whole reactor behaves closer to a continuous, well-mixed, tank reactor, the productivity is higher. This situation corresponds to a scheme with few, highly mixed sections modeling the bed: the larger the number of sections, the closer the behavior to that of a tubular reactor with poor back-mixing. Same effect produces decreasing the mixing factor with a minimum for $f_A = 0$.

In Figure 4, the corresponding pictures for the temperature and concentration of the gas leaving the bed in the form of bubbles are shown. Clearly, the same effects presented in previous paragraphs are observed here: a more realistic representation of the mixing conditions in a commercial reactor is associated to less sections and more back-mixing. Moderate to high levels of agitation are typical features in all fluidized bed reactors; the introduction of the mixing factor f_A is aimed at taking this fact into account in the model.

Considering both Figures 3 and 4, it can be observed that there is a direct relationship between the increase in the value of the mixing factor f_A and the growing reactor production and its associated temperature and monomer concentration. The effect, however, is not linear due to the thermal evolution related to polymerization via the Arrhenius type function driving the reaction kinetics.

Figure 5 shows the temperature distribution for solid particles along the bed height for several values of the mixing factor f_A. Reactor production is constant for all plots, and equal to 72 kilograms of polyethylene per hour and bed cubic meter. All curves show temperatures increasing with bed height, although a different behavior

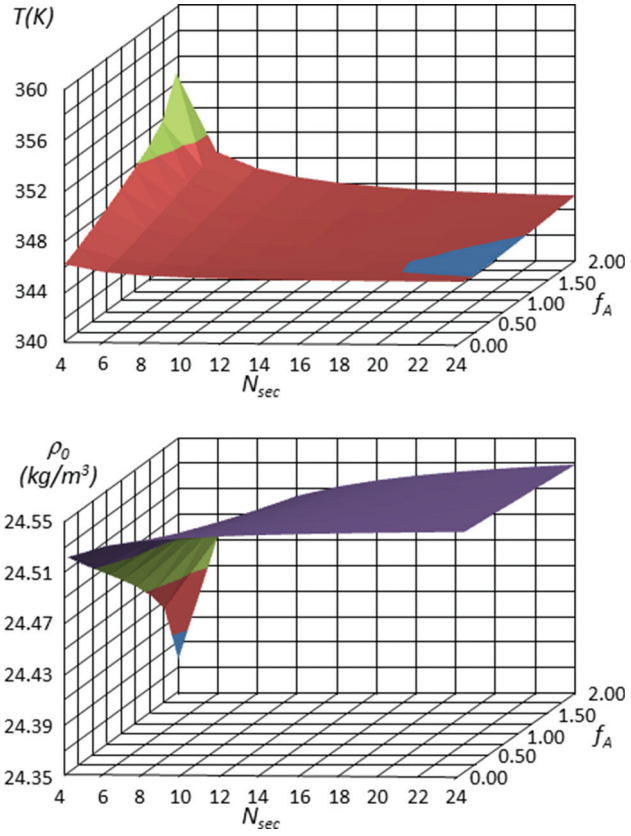

Figure 4: Bubble temperature (K) and ethylene concentration (kg/m^3) at top of the bed vs. number of sections and mixing factor, for $f_c = 1$.

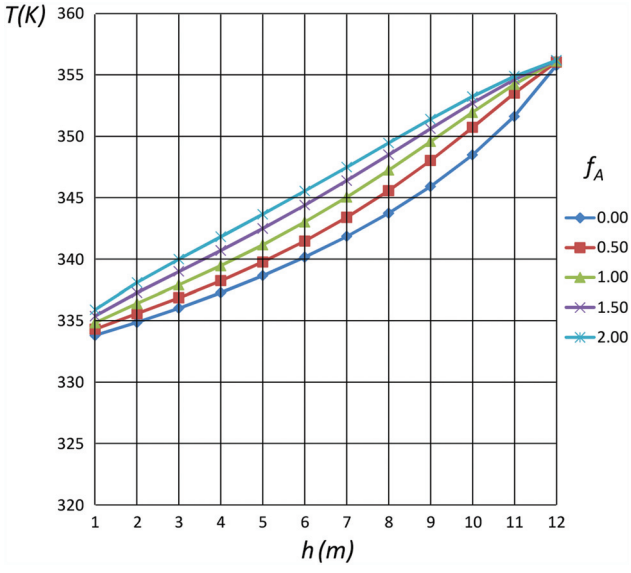

Figure 5: Solid particle temperature (K) vs. bed height and f_A, for productivity = 72 kg/h m^3.

is observed for them according to the f_A selected. If no axial mixing is present ($f_A = 0$) the temperature curve is monotonously increasing and its slope grows with the bed height. If a larger f_A is considered, the temperature curve behavior changes and for $f_A = 2$ an inversion of its concavity is observed.

Next, the model was used to explore the effect of the inlet gas velocity on the reactor operation. It was found that productivity suffers a notorious descent if said velocity is increased. Two factors are related to this effect: firstly, the residence time of the reactants decreases, thus reducing both the amount of polymer produced per unit time and per unit volume.

Additionally, the higher gas flow rate improves the heat transfer from the active sites towards the reactor exterior, producing a reduction of the particle temperature and consequently of the kinetic constant. In Figure 6, it can be seen that if the gas velocity at the bottom of the bed is changed from 0.50 to 0.90 m/s, polyethylene reactor production drops from 26.39 to 15.99 kg/h m^3 if $f_A = 0$, and from 49.21 to 16.64 kg/h m^3 if $f_A = 2$. These results show that the effect of the gas velocity is more evident when the degree of axial mixing is higher.

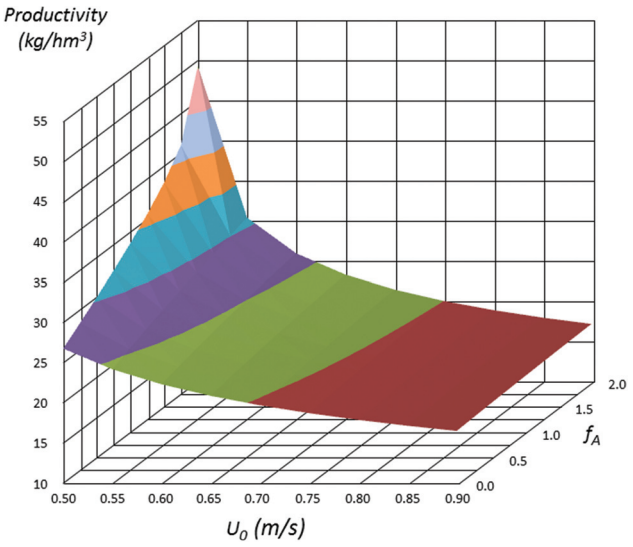

Figure 6: Polyethylene productivity (kg/h m^3) vs. inlet gas velocity and f_A.

The effect of u_0 on the temperature of the solid leaving the reactor is shown in Figure 7. It can be observed that, for $f_A = 2$, the solid temperature falls around 18.5 K when the velocity of the gas entering the reactor increases from 0.5 to 0.9 m/s. On the other hand, for $f_A = 0$ the drop is of approximately 8 K for the same gas velocity change.

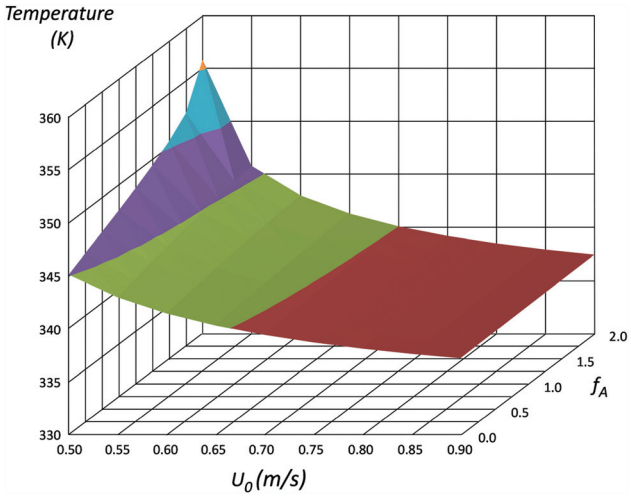

Figure 7: Solid particle temperature at bed top (K) vs. inlet gas velocity and f_A.

This behavior shows that, when axial mixing is important, the temperature is significantly affected by the gas velocity, with the observed decay in solid temperature mostly related to the impact higher levels of mixing have on the bed heat-transfer conditions.

The model was also used to explore the effect of changing the inlet gas temperature, in the understanding that this scouting should be limited to a relatively small domain, since too high the inlet gas temperature could present a serious difficulty to heat removal from the reactor. The exponential relationship in the Arrhenius type kinetic equation produces a considerable increase in polymerization even for relatively small changes in T_0. Figure 8 shows productivity values for several inlet temperatures and mixing factors f_A.

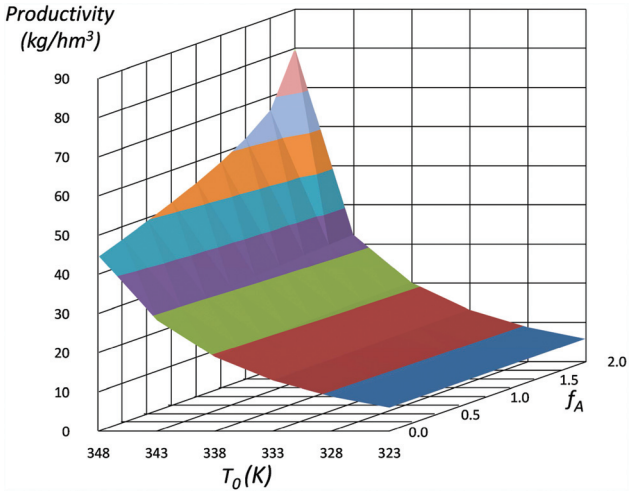

Figure 8: Polyethylene productivity (kg/h m^3) vs. inlet gas temperature and f_A.

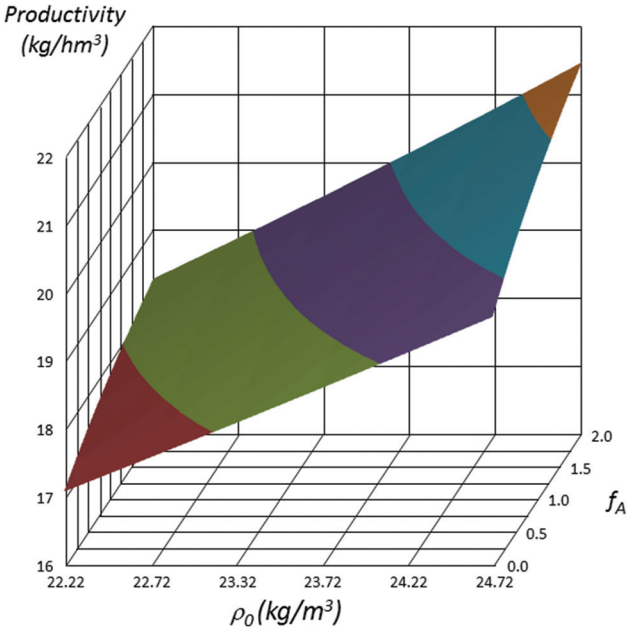

Figure 9: Polyethylene productivity (kg/h m^3) vs. inlet ethylene concentration and f_A.

The same analysis was performed in terms of changes in the monomer concentration in the gas fed to the reactor. In Figure 9, it can be observed that if said concentration is increased, the model predicts a growth in the amount of polymer produced per unit time and per unit volume. This is so due to the first order kinetics in the catalyst active sites that reacts enlarging the productivity if the monomer concentration is higher. A temperature increment is also present, contributing to add to the production increase.

The model combining the plug flow model for the gas streams (bubbles and interstitial gas) and a set of particles with various degrees of axial mixing, applied to the base-case study presented above, was used to analyze limiting steady-state conditions. Results show that when mixing effects increase, the system begins to express some inherent instability that impedes achieving high production values. This instability of the model had been already observed when computations were performed using the two-phase model (bubble and emulsion), which is the predecessor of the current three-phase scheme. Indications are that, as the behavior of the solid phase approaches that in a perfectly mixed model, instabilities appear. This fact precludes the establishing of an operating, steady-state point in the acceptable range of temperatures in the reactor. This situation has been analyzed scouting the onset of instabilities increasing the kinetic factor, whilst setting all other operating conditions (gas inlet temperature and compositions, gas velocity, average diameters of bubbles and particles, physical properties, etc.) at fixed values. The model was used gradually increasing the kinetic factor until instability occurs. Passed this point, the solutions obtained are physically unacceptable because they correspond to excessively high temperatures.

Figure 10 shows the surface with the values of the maximum attainable kinetic factor f_c that, for each pair of values of the parameters N_{sec} and f_A, is still in the stable region of the reactor operation. If higher values of f_c are used for said pair, the model shows instability. It can be observed that the minimum value of these limiting f_c (1.00) is found for the number of section equal to 4, the lower value used in the simulations. Additionally, said f_c corresponds to $f_A = 2$, the value representing the maximal degree of mixing analyzed in this work. Conversely, when the number of sections is 24, and no axial mixing is considered ($f_A = 0$), the operating condition for the reactor thus obtained is the one closer to that in a tubular reactor. The system shows stability and the higher value of f_c is observed (1.60) located on the left-hand, upper point of the surface in Figure 10.

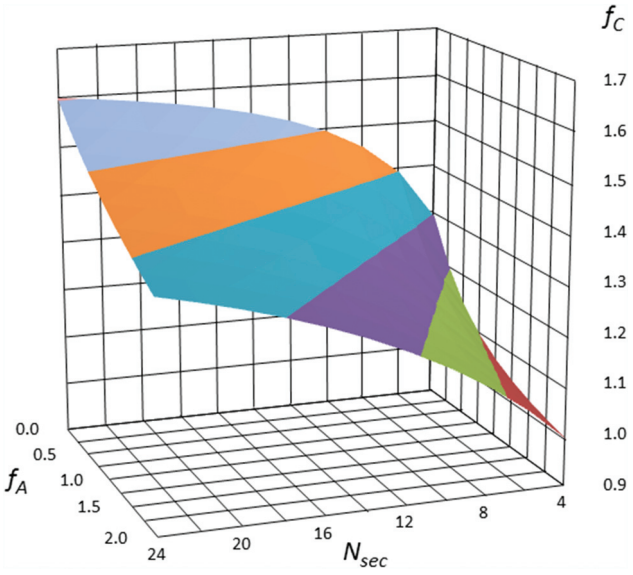

Figure 10: Maximum attainable kinetic factor f_c as function of *Nsec* and f_A for the stable reactor operation.

We conclude that, as model predictions approximate the conditions in a well-mixed bed, i.e. when a behavior closer to that in a CSTR is assumed, the instability situation is reached earlier. Hence, a limit for the value of the kinetic factor is found, not to be exceeded if acceptable operating conditions are desired. Consequently, when the number of sections into which the bed is divided increases, the maximum feasible value for the kinetic factor is higher, and this

is expressed through an increase in the reactor productivity. Additionally, the temperature of the solid shows a substantial increase due to the higher thermal evolution of the system associated with the augmented reaction rate. In this case, the overall reactor model approaches the behavior of a tubular reactor. When the value of f_A is used to analyze the effect of the degree of axial mixing in the solid phase, it is observed that increasing this factor the instability appears earlier, namely the limiting value of the kinetic factor is lower. Thus, the maximum output that can be achieved diminishes and so does the polymer temperature at the reactor outlet.

5 Conclusions

The model approaches a realistic representation of the reactor phases and accounts for, in a simple manner, the presence of solid back-mixing. The scheme differentiates the bubble gas from the interstitial emulsion gas, considering via f_A the complex particle-movement, with ascending trajectories by the entrainment of bubbles. The backflow so introduced changes traditional patterns in modeling the emulsion. High levels of mixing are proposed everywhere in the reactor, bringing the representation of their behavior closer to that in a CSTR. The presence of an inflection point in the concavity of the temperature profiles in Figure 5 is an indication of this change.

Handling the f_A parameter allows for approaching of the emulsion phase behavior to that in a series of well-mixed tanks but, because of the high L/D ratio, not so close as to show instabilities.

Acknowledgments: The authors acknowledge the financial support received from the National Research Council (CONICET) and Universidad Nacional del Litoral (UNL) through Project PIP 2008 – CONICET "Nuevos Desarrollos en la Síntesis de Polímeros del Estireno, el Formaldehído y el Etileno" and CAI + D 2009 – UNL "Polímeros del Etileno, del Ácido Acrílico y del Formaldehído de Interés Industrial". Also want to thank especially Dr. Pedro Morin (IMAL-UNL-CONICET) for their advice in the numerical solution of the problem.

Nomenclature

A_{sg}	area of solid-gas interface, m^2
A_T	cross area of the reConsejoactor, m^2
Cp_j	specific heat of the species i at a constant pressure, J/kg K
d_b	bubble diameter, m
d_p	particle diameter, m
D	diameter of the reactor, m
D_g	gas diffusivity, m^2/s
f_A	mixing factor
f_c	kinetic factor
g	acceleration of gravity, m/s^2
h	heat transfer coefficient between solid and gas, W/m^2 K
H_{big}	heat transfer coefficient per unit volume of bubble, W/m^3 K
k^s	reaction rate constant, 1/s
k_g	thermal conductivity of gas, W/m K
K_{big}	mass transfer coefficient per unit volume of bubble, m^2/s
L	fluidized bed height, m
L_S	height of the section under consideration, m
T	temperature, K
u_0	superficial gas velocity at the inlet, m/s
u_b	velocity of the bubble phase, m/s
u_{br}	relative velocity of the bubble, m/s
u_{mf}	minimum fluidization velocity, m/s

Greek symbols

δ	fraction of bubbles in the bed
ε	minimum fluidization porosity
μ_g	gas viscosity, Pa s
ρ_g	gas density, kg/m^3
ρ_{et}	mass concentration of ethylene in the gas, kg/m^3

Superscripts

i	input to the section considered
o	output from the section considered
^	refers to interstitial gas
–	refers to solid phase

References

1. Bortolozzi, R.A., Chiovetta, M.G., 2006. Modelado de un reactor de lecho fluidizado para la producción de polietileno. XXII Interamerican Congress of Chemical Engineering and V Argentinian Congress of Chemical Engineering. Buenos Aires. Argentina. Abstracts, 249.
2. Bortolozzi, R.A., Chiovetta, M.G., 2007. Modeling of mixing effects in a fluidized-bed for olefin polymerization. IV Simposio Chileno-Argentino de Polímeros – ARCHIPOL 2007, Viña del Mar, Chile. Abstract SP51-MM.
3. Bortolozzi, R.A., Chiovetta, M.G., 2010. Comparación de modelos de reactores de lecho fluidizado para la producción de poliolefinas usando condensables. VI Congreso Argentino de Ingeniería Química, CAIQ 2010, Mar del Plata, Argentina. Abstract ID 1082, 293. Full paper in CD of Proceedings of Congress.
4. Chiovetta, M.G., Bortolozzi, R.A., 2009. Modeling mixing effects in fluidized-bed, ethylene-polymerization reactors with condensing agents. 8th World Congress of Chemical Engineering, Montreal, Canadá. Abstract 9O2FL8. Full paper 00000923.
5. Choi, K., Ray, W., 1985. The Dynamic Behaviour of Fluidized-Bed Reactors for Solid Catalysed Gas Phase Olefin Polymerization. Chem. Eng. Sci. 40, 2261–2279.

6. Darton, R., LaNauze, J., Davidson, J., Harrison, D., 1977. Bubble Growth Due to Coalescence in Fluidised Beds. Trans. I. Chem. Eng. 55, 274–283.
7. Dompazis, G., Kanellopoulos, V., Touloupides, V., Kiparissides, C., 2008. Development of a Multi-Scale, Multi-Phase, Multi-Zone Dynamic Model for the Prediction of Particle Segregation in Catalytic Olefin Polymerization FBRs. Chem. Eng. Sci. 63, 4735–4753.
8. Grosso, W.E., Chiovetta, M.G., 2005. Modeling a Fluidized-Bed Reactor for the Catalytic Polymerization of Ethylene: Particle Size Distribution Effects. Lat. Am. Appl. Res. 35, 67–76.
9. Kaminsky, W., Renner, F., 1993. High melting Polypropenes by Silica-supported Zirconocene Catalysts. Macromol. Rapid Commun. 14, 239–243.
10. Jenkins, J.M. III, Jones, R.L., Jones, T.M., Beret, S., 1986. Method for fluidized bed polymerization. United States Patent, US 4,588,790. Date: May 13, 1986.
11. Kiashemshaki, A., Mostoufi, N., Sotudesh-Gharebagh, R., 2006. Two-Phase Modeling of a Gas Phase Polyethylene Fluidized Bed Reactor. Chem. Eng. Sci. 61, 3997–4006.
12. Kou, B., McAuley, K., Hsu, C.C., Bacon D.W., Yao, K.Z., 2005. Mathematical Model and Parameter Estimation for Gas-Phase Ethylene Homopolymerization with Supported Metallocene Catalyst. Ind. Chem. Eng. Res. 44, 2428–2442.
13. Kunii, D., Levenspiel, O., 1991. Fluidization Engineering. 2nd ed. Butterworth-Heinemann, Boston.
14. Lucas, A., Arnaldos, J., Casal, J., Puigjaner, L., 1986. Improved Equation for the Calculation of Minimun Fluidization Velocity. Ind. Eng. Chem. Process Des. Dev. 25, 426–429.
15. Mahecha-Botero, A., Grace, J.R., Elnashaie, S.S., Jim Lim, C., 2009. Advances in Modeling of Fluidized-Bed Catalytic Reactors: A Comprehensive Review. Chem. Eng. Commun. 196, 1375–1405.
16. McAuley, K., Talbot, J., Harris, T., 1994. A Comparison of Two-Phase and Well Mixed Models for Fluidized-Bed Polyetilene Reactors. Chem. Eng. Sci. 49, 2035–2045.
17. Reid, R.C., Prausnitz, J.M., Poling, B., 1987. The Properties of Gases and Liquids. McGraw Hill, New York.
18. Univation Technical Report, 2013. Unipol PE Process, http//www.univation.com.
19. Wakao, N., Kaguei, S., 1982. Heat and Mass Transfer in Packed Beds. Gordon & Breach Science Publishers, New York.